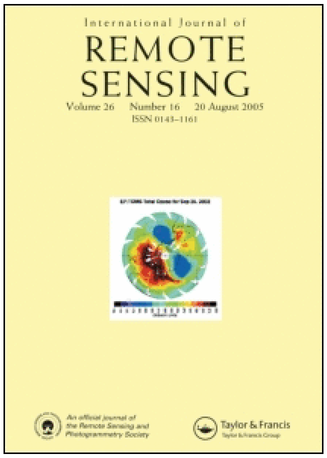

International Journal of Remote Sensing
Publication details, including instructions for authors and subscription information:
http://www.informaworld.com/smpp/title~content=t713722504

Evapotranspiration using MODIS data and limited ground observations over selected agroecosystems in India

Online Publication Date: 01 May 2007
To cite this Article: Mallick, K., Bhattacharya, B. K., Chaurasia, S., Dutta, S., Nigam, R., Mukherjee, J., Banerjee, S., Kar, G., Rao, V. U. M., Gadgil, A. S. and Parihar, J. S. , (2007) 'Evapotranspiration using MODIS data and limited ground observations over selected agroecosystems in India', International Journal of Remote Sensing, 28:10, 2091 - 2110
To link to this article: DOI: 10.1080/01431160600935620
URL: http://dx.doi.org/10.1080/01431160600935620

International Journal of Remote Sensing
Vol. 28, No. 10, 20 May 2007, 2091–2110

Taylor & Francis
Taylor & Francis Group

Evapotranspiration using MODIS data and limited ground observations over selected agroecosystems in India

K. MALLICK†, B. K. BHATTACHARYA*†, S. CHAURASIA†, S. DUTTA†, R. NIGAM†, J. MUKHERJEE‡, S. BANERJEE§, G. KAR¶, V. U. M. RAO**, A. S. GADGIL†† and J. S. PARIHAR†

†Agricultural Resources Group, Space Applications Centre (ISRO), Ahmedabad 380015, India

‡Department of Agronomy and Agricultural Meteorology, Punjab Agricultural University, Ludhiana 141004, India

§Department of Agricultural Meteorology, Bidhan Chandra Krishi Viswa Vidyalaya, Kalyani, Nadia 741235, India

¶Water Technology Centre for Eastern Region, Bhubaneshwar, India

**Department of Agricultural Meteorology, CCS Haryana Agricultural University, Hisar 125004, India

††Department of Geography, University of Pune, Pune 411007, India

(*Received 31 December 2005; in final form 3 May 2006*)

Plant growth processes and productivity of agroecosystems depend highly on evapotranspiration from the land (soil-crop cover complex) surface. A study was carried out using MODIS TERRA optical and thermal band data and ground observations to estimate evaporative fraction and daily actual evapotranspiration (AET) over agroecosystems in India. Five study regions, each covering a $10\,\text{km} \times 10\,\text{km}$ area falling in agricultural land use, were selected for ground observations at a time closest to TERRA overpasses. The data on radiation and crop parameters in paddy (irrigated and rainfed), cotton (rainfed), groundnut (residual moisture) crops were recorded at 14-day intervals between August 2003 to January 2004 from $2\,\text{km} \times 2\,\text{km}$ homogeneous crop patches within each study region. Eight MODIS scenes in seven optical (1, 2, 3, 4, 5, 6, 7) and two thermal bands (31, 32) level 1B data acquired from the National Remote Sensing Agency, Hyderabad, India and resampled at 1 km, were used to generate surface albedo (α), land surface temperature ($T_{\mathrm{s,\,MODIS}}$) and emissivity (ε_{s}). Evaporative fraction and daily AET were generated using a single source energy balance approach with (i) ground based observations only ('stand alone' approach), and (ii) 'fusion' of MODIS derived land surface variables on cloud free dates and coincident ground observations. Land cover classes were assigned using a hierarchical decision rule applied to multi-date Normalized Difference Vegetation Index (NDVI). The exponential model could be fitted between 1-$\mathrm{EF}_{\mathrm{ins,\,ground}}$ (ground based evaporative fraction) and difference between $T_{\mathrm{s,\,MODIS}}$ and air temperature (T_{a}) with R^2=0.77. Linear fit (R^2=0.74) could be obtained between 1-$\mathrm{EF}_{\mathrm{ins,\,ground}}$ and temperature vegetation dryness index (TVDI), derived from $T_{\mathrm{s,\,MODIS}}$-NDVI triangle. Energy balance daily AET from the 'fusion' approach was found to deviate from water balance AET by between 4.3% to 24.5% across five study sites

*Corresponding author. Email: bkbhattacharya@sac.isro.gov.in

International Journal of Remote Sensing
ISSN 0143-1161 print/ISSN 1366-5901 online © 2007 Taylor & Francis
http://www.tandf.co.uk/journals
DOI: 10.1080/01431160600935620

with a mean deviation of 11.6%. The root mean square error (RMSE) from the energy balance AET was found to be 8% of the mean water balance AET. The satellite based energy balance approach can be used to generate spatial AET, but needs more refinements before operational use in the light of progress in algorithms and their validation with huge datasets.

1. Introduction

The effect of water deficits on large agriculture is common as a result of deviations from normal rainfall pattern and non-availability of ground water or dam water for irrigation. This is one of the major constraints for biomass production at different growth stages and yield (Howell *et al.* 1998, Flexas *et al.* 2004). The ratio of actual evapotranspiration (AET) to potential evapotranspiration (PET) is an indicator of water deficit (1–AET/PET). A number of approaches are used to estimate PET from routine weather observations (Priestly and Taylor 1972, Doorenbos and Pruitt 1977). Actual evapotranspiration is generally measured in experimental fields using a lysimeter. However, the representative AET from lysimetric data for large areas is often non-satisfactory.

The estimation of actual evapotranspiration (AET) for a particular location can be made following two major approaches: (1) energy balance and (2) water balance. Its estimation over large agricultural patches was demonstrated using satellite optical and thermal data using (a) a vegetation index (VI) based empirical model (b) an energy balance physical model. Though VI based models (Nagler *et al.* 2005) are easy to use because of availability at relatively finer resolutions with high temporal frequency optical data as in MODIS 250 m, they need local calibration with ground measurements. On the other hand, the combined use of optical and thermal data results in direct quantification of AET through an energy balance model. The data from polar (NOAA AVHRR, MODIS TERRA and AQUA) orbiters with 1–2 acquisitions per day (Chen *et al.* 2005) and geostationary (GOES, METEOSAT, GMS) satellites with multiple acquisitions (Mecikalski *et al.* 1999) per day are generally utilized for this purpose. Most of the satellite-based energy balance approaches used a single source (Bastiaansen *et al.* 1998, Rosema 1993, Robeling *et al.* 2004) approach such as: SEBAL (Surface Energy Balance) or its modified form, METRIC (Mapping Evapotranspiration at High Resolution and with Internalized Calibration) (Allen *et al.* 2005) or a two-source (Norman *et al.* 1995, Chen *et al.* 2005) approach such as: ALEXI (Atmosphere Land Exchange Inversion) model.

The validation of satellite based instantaneous, hourly and daily evapotranspiration estimates generally calls for comparison of AET obtained from continuous ground based measurements of energy balance components such as: net radiation (Rn), sensible heat (H), ground (G) and latent heat fluxes (LE). The use of Bowen ratio or eddy covariance towers, with sufficient fetch (Anthoni *et al.* 2004), was demonstrated in different field campaigns for validating surface energy and water fluxes in FIFE (First International Satellite Land Surface Climatology Project Field Experiment) (Sellers *et al.* 1988, Hall *et al.* 1992), EFEDA (Echival Field Experiment in Desertification Threatened Area) (Bolle and Streckenbach 1993), Monsoon'90 (Kustas *et al.* 1994). The portable instruments for ground measurements could also be used for the preliminary evaluation of remote sensing based evapotranspiration estimates (Gupta and Sastry 1986).

Our present investigation aims at

(i) estimating AET with MODIS TERRA optical and thermal data, limited ancillary ground observations using an energy balance approach over five agroecosystems of India,
(ii) comparison of energy balance AET with soil water balance AET.

2. Study region and datasets

Eight cloud-free MODIS daytime (between 10:30–11:30 h local time) acquisitions from TERRA platform in 36 bands covering five study regions in different districts (Ludhiana, Punjab; Hisar, Haryana; Khurda, Orissa; Dhenkanal, Orissa; Nadia, West Bengal) distributed over four Indian states, were acquired. MODIS level 1B data products generated by NRSA, Hyderabad, India, resampled at 1 km spatial resolution in optical (1, 2, 3, 4, 5, 7) and thermal (31, 32) bands, were used. Fifteen sub-scenes from eight such scenes for the period August 2003 to January 2004 were extracted. The dimensions of sub-scenes were 105 rows $\times$ 92 columns (Punjab), 114 rows $\times$ 114 columns (Haryana), 186 rows $\times$ 226 columns (Orissa) and 273 rows $\times$ 236 columns (West Bengal), respectively. Five study regions, each of 10 km $\times$ 10 km area represent predominant cropping sequences of the area. Thus, each study region corresponds to 100 MODIS pixels within sub-scenes. Daily surface meteorological observations were available from all five stations. Diurnal observations on weather data at 12-s intervals were recorded by automatic weather stations (AWS) at Ludhiana and Khurda. Apart from weather observations, ground measurements on insolation, albedo, surface temperature, leaf area index were taken closest to MODIS overpasses at 14-day intervals in the 2nd and 4th week of each month between August 2003 to January 2004. Three replicated measurements were recorded with portable instruments at 500 m distance intervals within a 2 km $\times$ 2 km homogeneous crop patch centrally located within 10 km $\times$ 10 km study regions. The ground observation location patches were at Birmi ($30^\circ 50'$ N, $75^\circ 39'$ E): Ludhiana, Central State Seed Farm (CSSF) ($30^\circ 45'$ N, $75^\circ 42'$ E): Hisar, Jatni ($20^\circ 13'$ N, $85^\circ 42'$ E): Khurda, Bhuban ($20^\circ 52'$ N, $85^\circ 48'$ E): Dhenkanal, Ghetugachi ($23^\circ 03'$ N, $88^\circ 08'$ E): Nadia. Locations of AWS and surface meteorological observatories fall in study regions within 5 km radial distances from the central location of homogeneous patches. Details of study regions, dominant cropping sequences, ground and satellite data are presented in tables 1 and 2.

3. Methodology

3.1 *Pre-processing*

MODIS TERRA level 1B data were first corrected for bow-tie effects. Radiometric corrections to optical band data were carried out to remove atmospheric noises due to Rayleigh and molecular scattering, water vapour absorption. Sensor parameters, angular geometry and water vapour estimates (Sarvanaapavan *et al.* 1996) using split thermal channels (31, 32), were used for correction with 6S code (Vermote *et al.* 1997). Seven optical and two thermal (31, 32) bands were then georegistered for 15 sub-scenes.

3.2 *Surface energy balance computations*

The single source energy balance approach uses two different sources of datasets pertaining to

Table 1. Characteristics of homogeneous (2 km × 2 km) ground observation patch/site and datasets used.

Site (district)	Central latitude (N) longitude (E)	Cropping sequences	Growing season	Dates of MODIS subscenes	Dates of cloud free MODIS acquisitions coincident to ground observations
Birmi (Ludhiana)	30°45′ N 75°43′ E	Paddy (irrigated)	Monsoon	14 August 2003	
				26 August 2003	26 August 2003
				9 October 2003	9 October 2003
		Wheat	Winter	21 October 2003	
				27 November 2003	
CSSF (Hisar)	29°17′ N 75°42′ E	Cotton (partially irrigated)	Monsoon	14 August 2003	14 August 2003
				26 August 2003	
				9 October 2003	9 October 2003
		Wheat	Winter	21 October 2003	
				27 November 2003	
Jatni (Khurda)	20°12′ N 85°42′ E	Paddy (rainfed)	Monsoon	13 November 2003	13 November 2003
				26 November 2003	26 November 2003
Bhuban (Dhenkanal)	20°50′ N 85°50′ E	Groundnut (rainfed)	Winter	13 January 2004	13 January 2004
Ghetugachi (Nadia)	23°6′ N 88°2′ E	Paddy (irrigated)	Monsoon	26 November 2003	26 November 2003
		Paddy (irrigated)	Winter	13 January 2004	

(1) ground observations only
(2) MODIS data along with supplementary ground observations.

The ground based method, hereafter referred to as 'stand-alone', uses the means of replicated observations in a 2 km × 2 km homogeneous patch within the study region on instantaneous insolation, albedo, infrared thermometer surface temperatures at a time closest to MODIS TERRA overpasses, daily wind speed, leaf area index and crop height. These were converted to instantaneous energy balance components and evaporative fraction ($EF_{ins, ground}$). The second method is the 'fusion' of MODIS derived land surface variables such as: temperature ($T_{s, MODIS}$), Normalized Difference Vegetation Index (NDVI), albedo (α), and ancillary ground observations to generate instantaneous evaporative fraction ($EF_{ins, MODIS}$). The 2 × 2 pixel average of $T_{s, MODIS}$, NDVI and α, representing ground observation locations are used for the computations. The algorithms used in the 'fusion' approach are given below. The overall computational flow is given in figure 1.

3.2.1 Evaporative fraction. The proportion of moisture available for land (soil-crop cover complex) surface evaporation can be represented by evaporative

Table 2. Summary of ground observations.

Crop observations	Instruments/ techniques	Radiation observations	Instruments/ model/accuracy	Surface meteorological observations	Instruments/ techniques
Crop height (cm)	Measuring scale	Insolation/ surface albedo	Pyrano-albedometer (Kipp & Zonen SP LITE: $\pm 5\,\mathrm{W\,m^{-2}}$)	Maximum temperature (°C), minimum temperature (°C), maximum RH (%), minimum RH (%), wind speed ($\mathrm{m\,s^{-1}}$), bright sunshine hour (hrs)	IMD agrometeorological observatory as per WMO specifications
LAI	Canopy analyzer (LICOR : LAI 2050)	Photosynthetically active radiation (PAR)	Line quantum sensor (LICOR Sunscan)		
Soil moisture at 10 cm, 30 cm and 60 cm depth	Gravimetric sampling	Net radiation	Net radiometer (Kipp & Zonen NR LITE: $\pm 5\,\mathrm{Wm^{-2}}$)	Air temperature (°C), RH (%), wind speed ($\mathrm{m\,s^{-1}}$), insolation ($\mathrm{W\,m^{-2}}$) at 12 s interval (only for Ludhiana and Khurda)	Automatic weather station (METOS Instruments Pvt. Ltd)
Above ground biomass ($\mathrm{g\,m^{-2}}$)	Destructive sampling	Canopy temperature	Infrared thermometer (Telatemp : ± 0.2°C)		

fraction (EF).

$$\mathrm{EF_{ins,\,MODIS}} = \mathrm{LE_{ins,\,MODIS}} / \left(\mathrm{Rn_{ins,\,MODIS}} - \mathrm{G_{ins,\,MODIS}}\right) \tag{1}$$

where $\mathrm{Rn_{ins,\,MODIS}}$-$\mathrm{G_{ins,\,MODIS}}$ is the net available energy, $\Delta\mathrm{Q_{ins,\,MODIS}}$ ($\mathrm{W\,m^{-2}}$), $\mathrm{Rn_{ins,\,MODIS}}$ is the instantaneous net radiation ($\mathrm{W\,m^{-2}}$), $\mathrm{G_{ins,\,MODIS}}$ is the instantaneous ground heat flux ($\mathrm{W\,m^{-2}}$), $\mathrm{LE_{ins,\,MODIS}}$ is the instantaneous latent heat flux ($\mathrm{W\,m^{-2}}$) i.e. $\Delta\mathrm{Q_{ins,\,MODIS}} - \mathrm{H_{ins,\,MODIS}}$ and $\mathrm{H_{ins,\,MODIS}}$ is the instantaneous sensible heat flux ($\mathrm{W\,m^{-2}}$).

The computation of net available energy requires net radiation and ground heat flux to be computed. All the satellite based approaches are more or less similar for computing these two energy balance components, but largely differ in sensible heat flux computation which is the 'heart' of energy balance computations.

3.2.1.1 Sensible heat flux. The heat energy exchange between land surface and overlying air can be ascertained by sensible heat computation as given below. The differences in the present approach of sensible heat computation from an existing well-known approach, SEBAL/METRIC, are given in table 3.

$$H_{\mathrm{ins}}\left(\mathrm{W\,m^{-2}}\right) = \rho C_{\mathrm{p}}\left(T_{\mathrm{s,\,MODIS}} - T_{\mathrm{a}}\right) / \left(r_{\mathrm{ah}} + r_{\mathrm{ex}}\right) \tag{2}$$

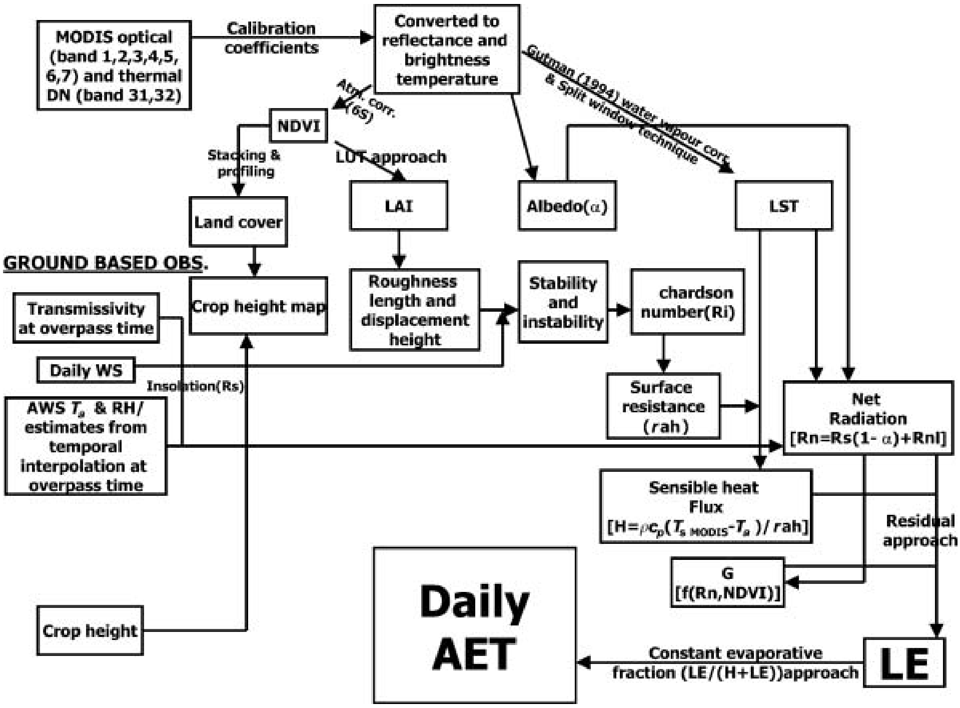

Figure 1. Computation flow of daily AET using the 'fusion' approach.

where ρ is the air density ($\mathrm{kg\,m^{-3}}$), C_p is the volumetric heat capacity ($\mathrm{J\,m^{-3}\,K^{-1}}$), r_{ah} is the aerodynamic resistance ($\mathrm{s\,m^{-1}}$) between land and atmosphere computed for both (a) stable and (b) unstable atmospheric conditions, r_{ex} is the extra resistance ($\mathrm{s\,m^{-1}}$) due to differences in roughness length for heat and momentum transfer.

ρC_{p} is approximately $1000\,\mathrm{J\,kg\,k^{-1}}$. $T_{\mathrm{s,MODIS}}$ (k) is land surface temperature (LST) estimated using the split window technique (Becker and Li 1990) with MODIS 31 and 32 thermal bands. T_{a} (K) is ground observed air temperature at the time of MODIS overpass. Measured air temperatures and relative humidity (RH) at overpass time obtained from AWS at Ludhiana and Khurda were used. Overpass time air temperatures at Hisar and Nadia were estimated using measurements on maximum, minimum air temperatures at surface observatory and sinusoidal function (Parton and Logan 1981). Similarly, relative humidity (RH) at MODIS overpass time was computed using observed $\mathrm{RH_{max}}$, $\mathrm{RH_{min}}$ and cosine function (Butler 1992).

$$r_{\mathrm{ah}} = (\ln((h_{\mathrm{t}} - d)/z_{\mathrm{oh}}) - \psi_{\mathrm{h}})(\ln((h_{\mathrm{u}} - d)/z_{\mathrm{om}}) - \psi_{\mathrm{m}})/(k^2 u) \tag{3}$$

ψ_{m}, ψ_{h} are atmospheric stability-unstability related parameters for momentum and heat transfer respectively.

Stabilty and unstability conditions are represented by Richardson number (R_{i}).

$$\begin{aligned} \mathrm{R_i} &= (\text{free convection}/\text{forced convection}) \\ &= g(T_{\mathrm{s,MODIS}} - T_{\mathrm{a}})(h_{\mathrm{t}} - d)/(T_{\mathrm{a}} u^2) \end{aligned} \tag{4}$$

Table 3. Major differences in instantaneous sensible heat computation (H_{ins}) with satellite and ground data between SEBAL/METRIC and the present algorithm.

Parameters	SEBAL/METRIC	Present algorithm
1. H_{ins}	$\rho C_p\ (dT/r_{ah})$	$\rho C_p\ (dT/r_{ah}+r_{ex})$
1.1 dT	(a) $a+bTs$, a and b are coefficients determined through iterative procedures while carrying out stability correction for computing aerodynamic resistance	(a) T_s-T_a
	(b) dT is the estimated difference between near surface (0.1 m) and 2 m above surface air temperatures. It compensates for problems caused by differences between radiometric and aerodynamic surface temperatures.	(b) extra resistance (r_{ex}) due to differences in roughness length for heat and momentum transfer. It compensates also for the difference between radiometric and aerodynamic surface temperatures (Kustas *et al.* 1989). $r_{ex}=\mathrm{kB}^{-1}/(0.4u_{star})$ kB^{-1}=ln(momentum roughness length/heat roughness length) u_{star}= frictional velocity
1.2 r_{ah}	(a) Stability correction was done by estimating Z/L using iterative procedure applying Monin-Obukhov similarity theory. It requires 'hottest' and 'coldest' pixels in a heterogeneous landscape, which may not occur particularly in large lowland rice agriculture and arid agriculture (Tasumi 2003). It may restrict the estimation of Z/L through iterative procedure.	(a) Stability correction was done by Richardson number (R_i) thresholds. The estimation of R_i is independent of surface heterogeneity in wetness pattern. Moreover, it requires the same number of surface and meteorological parameters as used to estimate Z/L.
	(b)The iterative procedure requires computation of instantaneous latent heat flux over hottest and wettest pixel in METRIC. It uses grass reference instantaneous ET computed from weather station data and it also assumes crop coefficient 0.0 and 1.05 for hottest and driest pixels, which may not be true	(b) No assumption on crop coefficient is required

(a) For stable conditions, R_i is taken to be more than 0.025 (Gupta and Sastry 1986)

$$\psi_m=\psi_h=-5\xi \tag{5}$$

$$\xi=R_i/(1-5R_i) \tag{6}$$

(b) For unstable conditions, R_i remains between −0.25 to 0.025

$$\psi_m=2\ln((1+x_i)/2)+\ln\left(\left(1+x_i^2\right)/2\right)-2\arctan(x_i)+\pi/2 \tag{7}$$

$$\psi_h=2\ln\left((1+x_i)^2\Big/2\right) \tag{8}$$

$$x_i=(1-16\xi)^{1/4} \tag{9}$$

$$\xi=R_i \tag{10}$$

$$r_{ex} = \mathrm{kB}^{-1}/(\mathrm{k}u_{star}) \tag{11}$$

$$\mathrm{kB}^{-1} = \ln(z_{om}/z_{oh}) \tag{12}$$

h_t is the height (m) of air temperature measurement=2.0 m, h_u is the height (m) of wind speed measurement=10.0 m, u is the wind speed (m s^{-1}) at the top of the canopy,

$$\begin{aligned} d &= \text{displacement height (m)} \\ &= h_t\left(1-\left(1-\exp\left(-(20.6\mathrm{LAI})^{1/2}\right)\right)\Big/\left((20.6\mathrm{LAI})^{1/2}\right)\right) \end{aligned} \tag{13}$$

$$\begin{aligned} z_{om} &= \text{roughness length for momentum transfer} \\ &= (h_t - d)/(\exp(k(1/\text{ratio}) - E_h)) \end{aligned} \tag{14}$$

$$\text{ratio} = u/u = (C_s + C_r\mathrm{LAI}/2)^{1/2} \tag{15}$$

$$\begin{aligned} C_s &= \text{drag coefficient for unobstructed bare soil} \\ &= k^2((\ln(h_t - d)/z_{oh}) + E_h) \end{aligned} \tag{16}$$

$$\begin{aligned} C_r &= \text{overstorey drag coefficient } (=0.35) \\ u^* &= \text{frictional velocity } \left(\mathrm{ms}^{-1}\right) = (k_u)/(\ln((h_u - d)/z_{om}) - \psi_m) \end{aligned} \tag{17}$$

$$E_h = \text{vegetation influence function} = \ln(C_w) - 1 + C_w^{-1} \tag{18}$$

C_w is the dimensionless constant (C_w=2.0)
z_{oh} is the roughness length (m) for heat transfer estimated from

$$\begin{aligned} &\mathrm{IF}\left((C_s + C_r\mathrm{LAI}/2)^{1/2} < 0.3,\ (h_t - d)\Big/\left(\mathrm{EXP}\ \left(\left(k/(C_s + C_r\mathrm{LAI}/2)^{1/2}\right) - \psi_h\right)\right),\right. \\ &\quad (h_t - d)/(\mathrm{EXP}((k/\text{ratio}) - \psi_h)) \end{aligned} \tag{19}$$

k is the Von Karman constant(=0.41), LAI is the leaf area index estimated from NDVI and land cover based look-up table for agricultural patches (Liang 2004).

3.2.1.2 Net available energy ($\Delta Q_{ins,\,MODIS}$*).*

$$\begin{aligned} \Delta Q_{ins,\,MODIS} &= \left(\mathrm{Rn}_{ins,\,MODIS} - \mathrm{G}_{ins,\,MODIS}\right) \\ \mathrm{Rn}_{ins} &= \mathrm{Rs}_{ins}(1-\alpha) + \left(\sigma\varepsilon_a\varepsilon_s T_a{}^4 - \sigma\varepsilon_s T_s{}^4\right) \end{aligned} \tag{20}$$

Where

$$\mathrm{Rs}_{ins} \text{ is the instantaneous insolation } \left(\mathrm{W\ m}^{-2}\right) = 1367\varepsilon t\cos(\theta) \tag{21}$$

$$\begin{aligned} \varepsilon &= \text{Duffe Backman constant for SunEarth distance correction} \\ &= 1.00011 + 0.34221\cos(\mathrm{da}) + 0.00128\sin(\mathrm{da}) + 0.000719\cos(2\mathrm{da}) \\ &\quad + 0.000077\sin(2\mathrm{da}) \end{aligned} \tag{22}$$

t is the atmospheric transmissivity obtained from ground measured insolation closest to MODIS TERRA pass, θ is the pixelwise solar zenith angle (radian) from MODIS data products.

$$\begin{aligned}\alpha = &\text{surface albedo using narrow band–to–broad band conversion as} \\ &\text{reported by Liang(2000)} \\ = &0.160\text{ref}1 + 0.291\text{ref}2 + 0.243\text{ref}3 + 0.116\text{ref}4 \\ + &0.112\text{ref}5 + 0.081\text{ref}7 - 0.0015\end{aligned} \tag{23}$$

da is the day angle (radian), ref1 to ref7 represent surface reflectances in MODIS bands from 1 to 7.

$$\varepsilon_s = 1.009 + 0.047^{*}\text{ALOG(NDVI)} \quad \text{(Van de Griend and Owe 1993)} \tag{24}$$

NDVI is equal to (ref2-ref1)/(ref2+ref1). ε_a is the air emissivity estimated using ground air temperature (T_a in °C),

RH at MODIS TERRA overpass time and Brutsaert (1975) equation

$$\begin{aligned}\text{G}_{\text{ins}} = &\text{instantaneous ground heat flux } \left(\text{W m}^{-2}\right) \\ = &\text{Rn}_{\text{ins}}((T_s - 273)/\alpha)\left(0.0032(1-\alpha) + 0.0062(1.1\alpha)^2\right) \\ &\left(1 - 0.978\text{NDVI}^4\right)(\text{Bastiaansen } et\ al.\ 1998)\end{aligned} \tag{25}$$

3.2.2 Conversion of evaporative fraction into daily actual evapotranspiration (AET).

$$\text{AET}\ \left(\text{mm day}^{-1}\right) = \text{EF}_{\text{day}}\left(\text{Rn}_{\text{day}}\right)/28.588 \tag{26}$$

EF_{day} is the daily evaporative fraction. Assuming evaporative fraction (Bastiaanssen *et al.* 1998) remains almost constant throughout the day,

$\text{EF}_{\text{day}} = \text{EF}_{\text{ins}}$:

$$\text{Rn}_{\text{day}} = \text{daily net radiation } \left(\text{W m}^{-2}\right) = (1 - c_1\alpha)\text{Rs}_{\text{day}} + \text{Rnl}_{\text{day}} \tag{27}$$

c_1 is the factor (1.1) for converting instantaneous albedo (α) to daily value, Rs_{day} is the daily average insolation (W m^{-2}) computed from station sunshine hours and daylength, Rnl_{day} is the daily average net longwave radiation (W m^{-2}) computed from station daily average air temperature ($T_{a_{avg}}$) and humidity (RH_{avg}).

4. Results and discussion

4.1 *Evaporative fraction (EF)*

Evaporative fraction represents relative moisture status of root zone. Attempts were made to relate instantaneous evaporative fraction ($\text{EF}_{\text{ins, ground}}$) derived from 'stand alone' approach to surface-air temperature difference (SATD is the $T_{s,\text{MODIS}}$-air temperature) and MODIS derived dryness index. Here, air temperature is at the time of MODIS TERRA pass obtained from weather observations closest to ground observation locations.

Table 4. Ground based energy balance components at TERRA overpasses over five observation patches.

Date	Site	Crop	Energy Balance components ($W m^{-2}$) using 'stand alone' approach			
			Rn	*G*	*H*	LE
26 August 2003	Birmi	Paddy	640	49	−15	606
9 October 2003	Birmi	Paddy	372	45	9	318
14 August 2003	CSSF	Cotton	619	27	57	535
9 October 2003	CSSF	Cotton	379	46	111	223
13 November 2003	Jatni	Paddy	485	51	79	355
26 November 2003	Jatni	Paddy	501	73	16	412
13 January 2004	Bhuban	Groundnut	460	93	83	284
26 November 2003	Ghetugachi	Paddy	411	31	35	345

4.1.1 Evaporative fraction and surface-air temperature difference (SATD). The instantaneous energy balance components, Rn (net radiation), *G* (ground heat flux), *H* (sensible heat flux), LE (latent heat flux), from coincident eight cloud free ground observation datasets closest to TERRA overpasses are given in table 4. Respectively, these varied from 372–620 $W m^{-2}$, 27–93 $W m^{-2}$, −15.0–111 $W m^{-2}$ and 284–586 $W m^{-2}$. Instantaneous evaporative fractions ($EF_{ins, ground}$) computed from the 'stand alone' approach using these eight datasets were plotted with SATD, which decreases with an increase in evaporative fraction showing curvilinear trend (figure 2). The exponential (R^2=0.77) model was fitted between SATD and 1-$EF_{ins, ground}$. While evaluating temporal variability of the evaporative fraction in a tropical watershed located in Naivasha basin, Kenya, inverse exponential relations were found by Farah *et al.* (2004) between evaporative fraction and SATD. Surface-air temperature difference is an indicator of a deficit in evapotranspiration (Hatfield *et al.* 1985, Moran *et al.* 1994) demand over the cropped area. This deficit is less with more moisture in the root zone. Actual evapotranspiration can be estimated by the statistical relation with Rn and SATD for different SATD limits (Seguin and Itier 1983). Thresholds of stress degree days (SDD) were suggested by Idso *et al.* (1981) for irrigation scheduling of different crops based on infrared thermometer observations in different growing conditions.

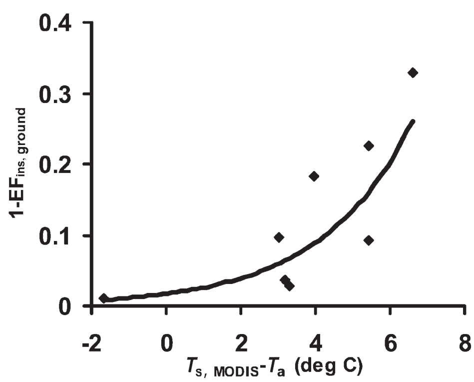

Figure 2. Relationship between evaporative fraction and surface air temperature difference. $y=0.0172e^{0.4118x}$, $R^2=0.77$.

The estimation of evaporative fraction from SATD using statistical relations can be used further for characterizing agriculture root zone moisture status, which is also input to different productivity models. The empirical models used to estimate volumetric soil moisture of root zone from SEBAL (Bastiaanssen *et al.* 1998) evaporative fraction are already incorporated in AHAS (Parodi 2000). This relation could be fine tuned with more datasets for general applications to agroecosystem monitoring in India.

4.1.2 Evaporative fraction and temperature vegetation dryness index (TVDI). This section explores the possibility of estimating evaporative fraction using MODIS land surface temperature ($T_{s,\mathrm{MODIS}}$) and NDVI values. A strong negative relationship was observed by Nemani *et al.* (1993) between surface temperature (T_s) and NDVI over all vegetation cover types. The similarity of T_s/NDVI relationships over different vegetation surfaces indicated that the fraction of vegetation cover and soil moisture status has a strong influence on the spatial variability of T_s. A substantial change in the T_s/NDVI relationship was found between wet and dry days for different fractional vegetation cover conditions. No change was observed over irrigated crops.

The triangular variant of $T_{s,\mathrm{MODIS}}$ and NDVI trapezoidal scatter was used to derive a dryness index called TVDI (Sandholt *et al.* 2002), which was similar to the CWSI (Crop Water Stress Index) concept given by Jackson *et al.* (1981).

$$\mathrm{TVDI} = \left(T_{s,\mathrm{MODIS}} - \left(T_{s,\mathrm{MODIS}}\right)_{\min}\right) / \left(\left(T_{s,\mathrm{MODIS}}\right)_{\max} - \left(T_{s,\mathrm{MODIS}}\right)_{\min}\right) \quad (28)$$

Where, $(T_{s,\mathrm{MODIS}})_{\max}$, $(T_{s,\mathrm{MODIS}})_{\min}$ were computed from the dry and wet edges respectively of the $T_{s,\mathrm{MODIS}}$ - NDVI triangle using linear relations with NDVI. $T_{s,\mathrm{MODIS}}$ is the current surface temperature in each pixel. TVDI outputs were generated from $T_{s,\mathrm{MODIS}}$ and NDVI for eight clear sub-scenes using their triangular relationship. The $T_{s,\mathrm{MODIS}}$ - NDVI scatters over Orissa and Ludhiana on 13 January 2004 and 9 October 2003 are shown in figure 3(*a*) and (*b*), respectively. The scatter over Orissa (figure 3(*a*)) is an ideal example of a triangle with uniform lower and upper boundaries forming a 'wet edge' and 'dry edge' respectively. The intermediate lines represent the T_s-NDVI relations for different cover types. The scatter deviates from the ideal triangle to become more trapezoidal in nature in Ludhiana (figure 3(*b*)). On other dates, the T_s-NDVI space showed deviations (other scatters not shown) from the ideal triangle in different agroclimatic regions though the scatter maintained dry and wet boundaries. The deviations from triangular scatter depend on the surface heterogeneity in cover types, wetness, growth stages, soil types, the size of sample subset considered to draw the scatter. A shifting window of uniform size was used by Nemani *et al.* (1993) to derive distributed surface wetness from T_s-NDVI inverse relations in an automatic mode. The empirical linear relations to estimate $(T_{s,\mathrm{MODIS}})_{\max}$ and $(T_{s,\mathrm{MODIS}})_{\min}$ from NDVI are shown in table 5. An example of distributed TVDI over Orissa is shown in figure 3(*c*).

The seasonal variation of TVDI during the crop growth cycle closely follows wetness-dryness cycles imposed by rainspells (Goward *et al.* 2002). This index was also used to derive surface soil (0–5 cm) moisture status (Wang *et al.* 2004). Since the evaporative fraction represents the root zone moisture status (Vogt *et al.* 2001, Scott *et al.* 2003), the relation of TVDI with it may exist. Bhattacharya *et al.* (1997) has already shown relations between surface and root zone moisture content in upland soils of northeastern India for monsoon, pre- and post-monsoon seasons. TVDI

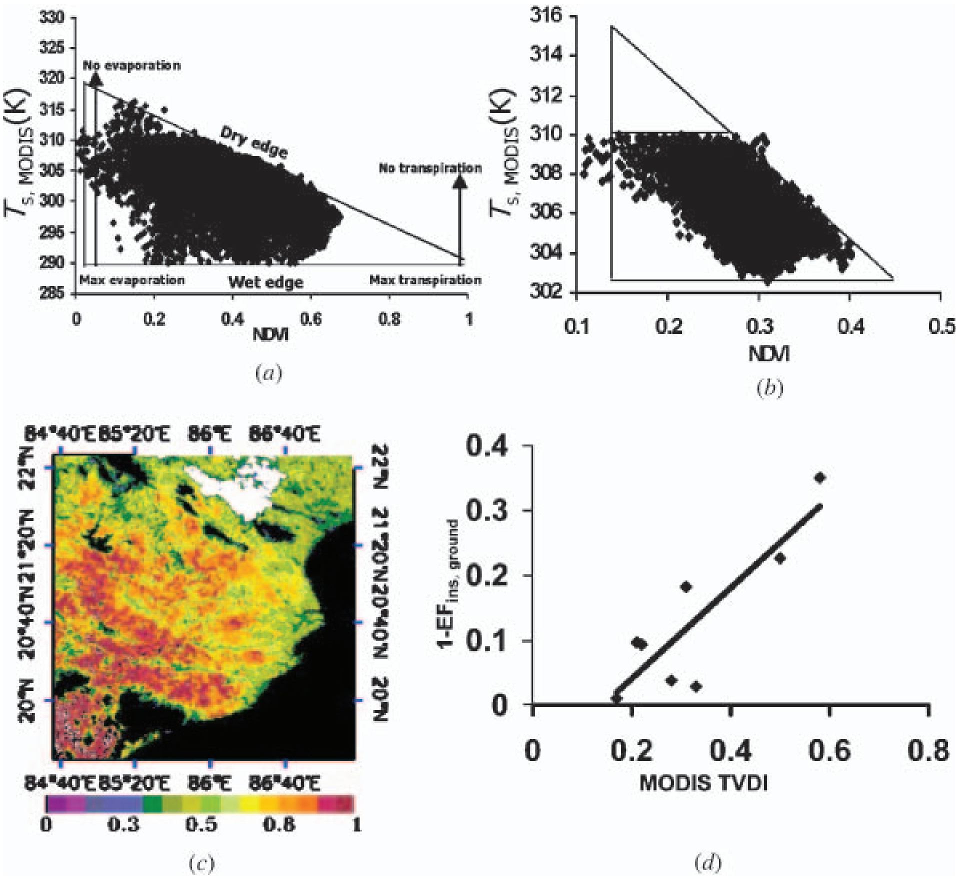

Figure 3. (*a*) LST-NDVI triangle over Orissa on 13 January 2004. (*b*) LST-NDVI triangle over Punjab on 9 October 2003. (*c*) temperature vegetation dryness index (TVDI) over Orissa on 13 January 2004. (*d*) Relationship between evaporative fraction and TVDI. $y=0.6986x-0.0992$, $R^2=0.74$.

averaged over 2×2 pixels encompassing the ground observation location patch were plotted with 1-EF$_{ins,\,ground}$ (figure 3(*d*)). A linear fit ($R^2=0.74$) could be obtained with offset on the *x*-axis. This relation clearly showed that dryness in the surface soil increases proportionally to dryness in the soil profile (surface to effective root zone) after a certain magnitude of surface soil moisture content has been depleted. The extrapolation of the earlier approach of estimating evaporative fraction from

Table 5. Empirical equation to derive $(T_{s,\,MODIS})_{max}$ and $(T_{s,\,MODIS})_{min}$ as a function of NDVI.

Date	Site	$(T_{s,\,MODIS})_{max}$	$(T_{s,\,MODIS})_{min}$
26 August 2003	Birmi	−13.712NDVI + 313.51	1.6581 NDVI + 299.33
9 October 2003	Birmi	−40.656 NDVI + 320.56	305.0
14 August 2003	CSSF	−32.527 NDVI + 326.4	304.7
9 October 2003	CSSF	−50.756 NDVI + 333.75	304.1
13 November 2003	Jatni	−33.602 NDVI + 321.84	−21.386 NDVI + 310.04
26 November 2003	Jatni	−23.242 NDVI + 314.32	−18.113 NDVI + 308.26
13 January 2004	Bhuban	−32.527 NDVI + 321.77	−11.788 NDVI + 303.52
26 November 2003	Kalyani	−20.153 NDVI + 311.39	−33.602 NDVI + 321.84

SATD will suffer if air temperature at overpass time is not available from a dense network of weather stations. However, the statistical relation based on TVDI can be extrapolated to a larger area to estimate evaporative fraction using satellite data only. The relation can be tuned up incorporating more datasets from different agroecosystems.

4.2 *Actual evapotranspiration (AET)*

4.2.1 Simulation of seasonal water balance AET. Soil-Water-Atmosphere-Plant (SWAP), a deterministic agrohydrological model, is used to simulate water balance AET from actual crop transpiration (AT) and actual soil evaporation (AE) during a crop growth cycle. The calibrated SWAP model was further used by Van Dam and Mallick (2003) in India to simulate water balance components in several crops such as wheat, paddy, cotton, grown in farmers' fields.

The potential evapotranspiration (PET) was computed from Priestly and Taylor's (1972) formulation using daily insolation, average air temperature, humidity and wind speed. PET is partitioned into potential evaporation (PE) and potential transpiration (PT) using periodic crop cover from leaf area index (LAI) and crop specific radiation extinction coefficient. PE was converted to AE based on surface soil moisture status updated every day after computing inflow (rainfall, irrigation) and outflow (run-off, deep percolation) components. Potential transpiration (PT) is converted to actual transpiration (AT) based on soil water fluxes available at the root zone. Apart from daily weather data, the crop and soil related state variables, which are inputs to SWAP, were collected from periodic field observations. The data pertaining to state variables used for SWAP runs and their sources of availability are listed in table 6.

The seasonal variation of daily rainfall, simulated daily AE and AT during growth cycles of paddy, cotton and groundnut at five observation patches is given in figure 4(*a*)–(*e*). The seasonal consumptive water use ($=\Sigma AE+\Sigma AT$) was highest for cotton (397.6 mm) at CSSF, Hisar followed by rainfed paddy (381.1 mm) at Jatni, Khurda, fully irrigated paddy (342.8 mm) at Birmi, Ludhiana, less irrigated paddy (241.4 mm) at Ghetugachi, Nadia and groundnut (140.4 mm) grown on residual moisture at Bhuban, Dhenkanal. Generally, the average crop water requirement is higher in cotton (700–1300 mm) than paddy (500–800 mm) followed by groundnut (Allen *et al.* 1998). The rainfed paddy, having longer growth duration (table 4), showed more consumptive water use than irrigated paddy.

4.2.2 Comparison of energy balance and water balance AET. The daily AET rates were computed from the evaporative fraction estimated from energy balance components using the 'fusion' approach on eight dates over five locations. These were compared with the water balance daily AET outputs from SWAP runs. The comparison (table 7) showed that the percentage absolute deviation of energy balance AET estimates from SWAP AET varied between 4.3% to 24.5% with a mean of about 11.6%. The root mean square error (RMSE) was found to be about 8% of the simulated mean AET over the dates of comparison. Energy balance AET was overestimated (figure 5) with respect to water balance AET on all eight dates. In the present study, a single source energy balance approach was used. Current validation results by French *et al.* (2005) regarding energy flux components with ASTER data over the SMACEX site showed that a two-source energy balance approach (TSEB) produces better AET estimates than a single source approach

Table 6. SWAP inputs used as state variables for soil water balance simulation.

Parameters	Site/ crop					Source
	Birmi/ Paddy	CSSF/ Cotton	Jatni/ Paddy	Bhuban/ Groundnut	Ghetugachi/ Paddy	
1. Growing period (days)	147	170	168	138	129	Phenological observations
2. Extinction coefficient						Computed from fortnightly radiation observations
(a) Direct light	0.25	0.70	0.30	0.35	0.30	
(b) Diffuse light	0.35	0.80	0.35	0.40	0.35	
3. Biometric parameters						Periodic observations
(a) Maximum Leaf Area Index (LAI)	4.7	2.0	4.1	4.7	8.3	
(b) Maximum crop height (cm)	80	110	100	50	100	
(c) Maximum root depth (cm)	75	100	75	45	95	
4. Minimum canopy resistance ($m\,s^{-1}$)	15	10	10	15	15	Computed from periodic observations
5. Maximum thickness of ponding water layer (cm)	6	0	5	0	7	Ground information
6. Residual moisture content ($cm^3 cm^{-3}$)	0.09	0.08	0.08	0.1	0.08	Ground information
7. Saturated moisture content ($cm^3 cm^{-3}$)	0.40	0.35	0.35	0.30	0.58	Ground information
8. Saturated hydraulic conductivity ($cm\,d^{-1}$)	38.3	35.3	35.0	20.7	43.7	Genutchen (1980)
9. Soil texture Sand:Silt:Clay (%)	Sandy loam 55:33:12	Sandy loam 75:12:13	Sandy loam 43:20:37	Sandy clay loam 39:24:37	Silt clay 8:68:24	Ground information
10. Soil profile depth (cm)	150	150	100	58	130	Ground information
11. Depth of impervious layer (cm)	180	200	90	65	180	Ground information
12. Irrigations						Ground information
(a) Number	18	1	0	0	6	
(b) Amount (cm)	5 each	7	0	0	6 each	

(SEBAL). Most of the disagreements between TSEB and SEBAL estimates were over sparsely vegetated sites, suggesting that the soil-vegetation differentiation accommodated by TSEB is a significant model benefit. The efficiency of simulating daily AET from the SWAP model was reported to be between 0.8–0.95 over a wide range of agroclimatic conditions across a variety of crops. Jiang *et al.* (2004) reviewed the efficiency of different satellite remote sensing based AET estimation methods and found that RMSE varied between 5–25% under different growing

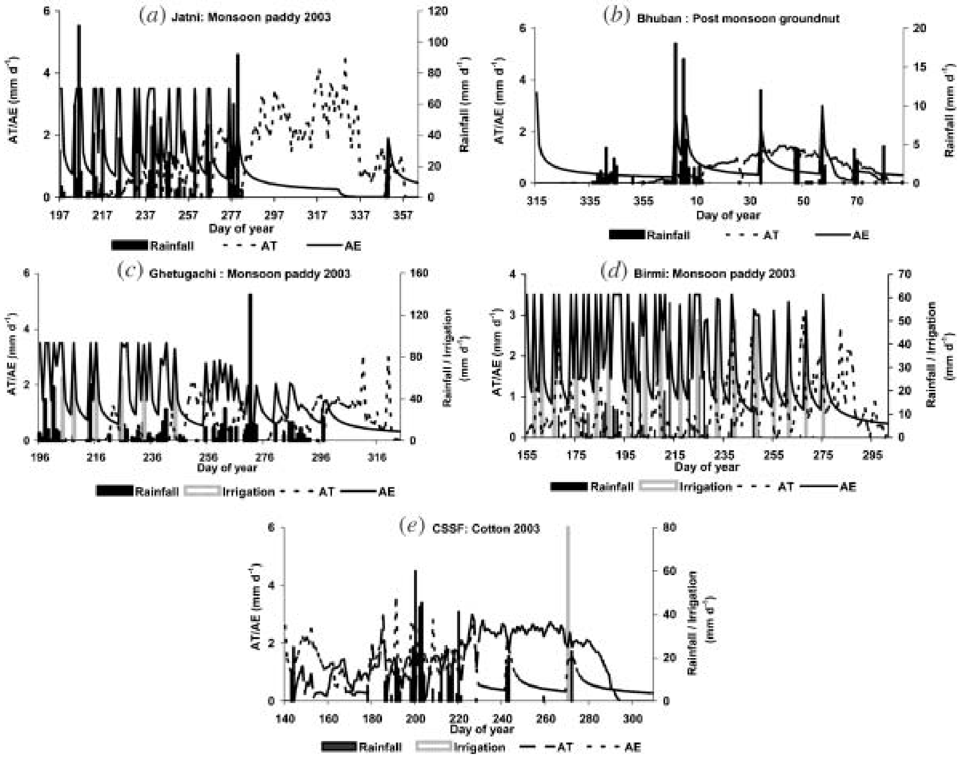

Figure 4. Major water balance components of SWAP model over five ground observation patches. (*a*) Jatni: monsoon paddy 2003, (*b*) Bhuban: post monsoon groundnut, (*c*) Ghetugachi: monsoon paddy 2003, (*d*) Birmi: monsoon paddy 2003, (*e*) CSSF: cotton 2003.

conditions. Nourbaeva *et al.* (2003) computed daily evapotranspiration from NOAA AVHRR surface temperature and NDVI over the Natori river basin and compared it with water balance AET. The deviation between AVHRR and water balance AET was of the order of 10–15%.

Table 7. Comparison of soil water balance and energy balance actual evapotranspiration (AET).

Site	Crop/date	MODIS AET ($mm\,d^{-1}$)	Water Balance (SWAP) AET ($mm\,d^{-1}$)	Absolute percent deviation (%)
Birmi	Paddy/			
	26 August 2003	7.0	6.5	6.5
	9 October 2003	3.5	3.3	4.9
CSSF	Cotton/			
	14 August 2003	6.3	5.6	10.0
	9 October 2003	3.1	2.3	24.5
Jatni	Paddy/			
	13 November 2003	4.4	4.1	6.6
	26 November 2003	4.7	4.5	4.3
Bhuban	Groundnut/			
	13 January 2004	2.2	1.8	14.4
Ghetugachi	Paddy/			
	13 November 2003	4.5	3.5	21.5

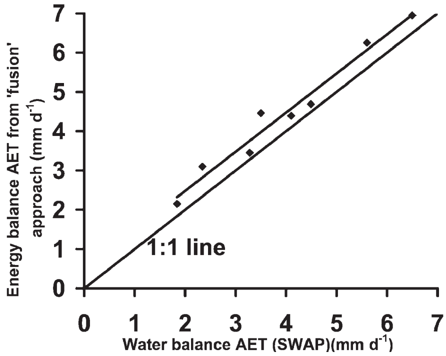

Figure 5. Comparison of energy and water balance actual evapotranspiration (AET). $y=0.9956x+0.4911$, $R^2=0.97$.

4.3 *Distributed outputs*

The generation of distributed energy balance outputs as well as $EF_{ins,\ MODIS}$ from MODIS data requires ground based information on distribution of crop height, wind speed, transmissivity of cloud free atmosphere and air temperature at satellite overpasses. The operational energy balance and AET algorithm of EARSL, Netherlands (Rosema 1993) with Meteosat data uses temporally varying but spatially constant transmissivity and wind speed in Africa, China and Europe. In this study, the distributed crop height was generated by assigning heights to crop cover classes. Pixel-wise air temperature was generated using the TVX method (Goward *et al.* 2002) using LST and NDVI through a shifting window of 9×9 pixels over sub-scenes. The transmissivity and wind speed measured near ground observation locations were kept spatially constant. However, the instantaneous insolation varies pixel wise based on solar zenith angle. The examples of distributed outputs on instantaneous net available (Rn-G) energy and evaporative fraction ($EF_{ins,\ MODIS}$) over agricultural surfaces in Orissa state on 13 November 2003 are shown in figure 6(*a*) and (*b*).

5. Conclusions

The advantage and value of MODIS data is to obtain a spatial representative measure of large areas. The individual measurements based on ground observations represent a point while the MODIS data help to quantify the spatial variation. Attempts were made for the first time in India to find out statistical relations between MODIS SATD and ground measured evaporative fraction or MODIS TVDI and evaporative fraction using the data from five different agroecosystems. These relations would be helpful to extrapolate to larger areas. Moreover, the outputs of daily evapotranspiration from the energy balance approach using the integration of MODIS data and ground observations were validated with daily AET from the well-calibrated water balance simulation model. The technique of the generation of distributed outputs of net available energy and evaporative fraction is also demonstrated in this study. Basically these two are needed to convert to daily distributed AET output. The future aim is to compare different satellite ET estimation techniques and accuracy evaluation by comparing with continuous diurnal measurements throughout the year using Bowen ratio towers at different

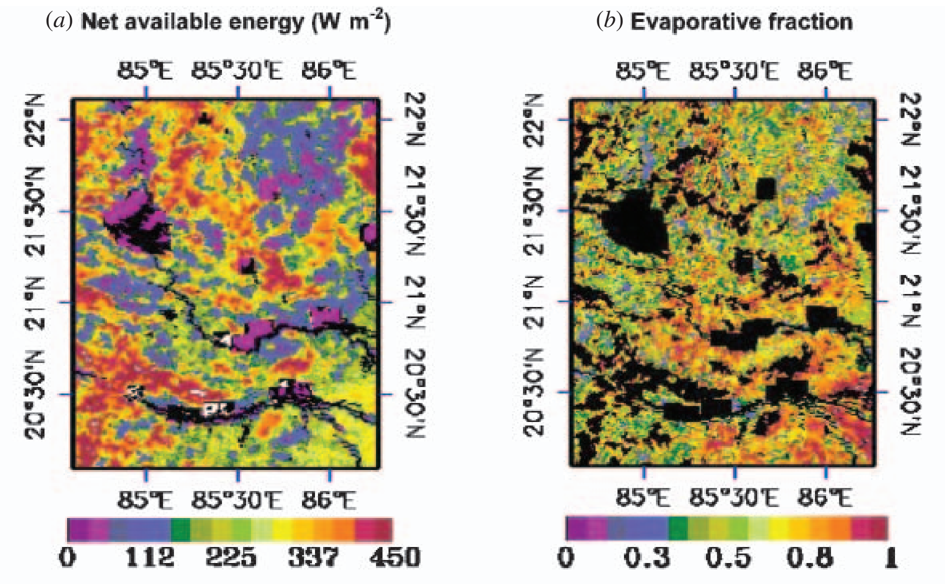

Figure 6. Distributed outputs of (*a*) net available energy and (*b*) evaporative fraction over a subscene (186 rows × 226 columns) in Orissa on 13 November 2003.

agroclimatic zones in India. The estimates of distributed evaporative fraction and evapotranspiration at a regional scale would be improved by incorporating interpolated weather variables such as: air temperature, humidity, insolation measured diurnally in a network of automatic weather stations (AWS).

Acknowledgments

The authors are highly grateful to Dr N. K. Patel, Head, Crop Inventory and Modelling Division for his valuable suggestions while carrying out the analysis. We are thankful to National Remote Sensing Agency (NRSA), Hyderabad, India for providing satellite data.

References

Allen, R.G., Pereira, L.S., Raes, D. and Smith, M., 1998, Crop evapotranspiration *FAO irrigation and drainage paper No. 56*, United Nations Food and Agriculture Organisation, Rome, Italy.

Allen, R.G., Tasumi, M. and Trezza, R., 2005, METRIC: Mapping Evapotranspiration at High Resolution- Applications Manual for Landsat satellite imagery. University of Idaho, 130 pp.

Anthoni, P.M., Freibauer, A., Kolle, O. and Schulze, E., 2004, Winter wheat carbon exchange in Thuringia, Germany. *Agricultural and Forest Meteorology*, **121**, pp. 55–67.

Bastiaanssen, W.G.M., Meneti, M., Feddes, R.A. and Holstag, A.A.M., 1998, A remote sensing surface energy balance algorithm for land (SEBAL) 1.Formulation. *Journal of Hydrology*, **212–213**, pp. 198–212.

Becker, F. and Li, Z.L., 1990, Towards a local split window method over land surface temperature from a satellite. *International Journal of Remote Sensing*, **11**, pp. 369–394.

Bhattacharya, B.K., Mitra, S. and Datta, M., 1997, Identification of water deficit and surplus periods and prediction of profile water content from surface soil water status in uplands of Tripura. *Journal of Indian Society of Soil Science*, **45**, pp. 698–701.

BOLLE, H.J. and STRECKENBACH, B. (Eds), 1993, *Flux estimates from remote sensing*, The Echival Field Experiment in a Desertification Threatened Area (EFEDA) final report, Berlin, August, pp. 406–424.

BRUTSAERT, W., 1975, On the derivable formula for long-wave radiation from clear skies. *Water Resources Research*, **11**, pp. 742–744.

BUTLER, D.R., 1992, Daily patterns of dew-point temperature in a semiarid climate. *Agricultural and Forest Meteorology*, **60**, pp. 267–278.

CHEN, Y.H., LI, X.B., LI, J., SHI, P.J. and DOU, W., 2005, Estimation of daily evapotranspiration using a two-layer remote sensing model. *International Journal of Remote Sensing*, **26**, pp. 1755–1762.

DOORENBOS, J. and PRUITT, W.O., 1977, Guidelines for Predicting Crop Water Requirements Irrigation and Drainage Paper 24, 2nd edn, FAO, Rome, 114 pp.

FARAH, H.O., BASTIAANSSEN, W.G.M. and FEDDES, R.A., 2004, Evaluation of the temporal variability of the evaporative fraction in a tropical watershed. *International Journal of Applied Earth Observation*, **5**, pp. 129–140.

FLEXAS, J., BOTA, J., CIFRE, J., ESCALONA, J.M., GLAMES, J., GULIAS, J., LEFI, E., FLORINDA, S., MARIA, M., MORENO, J., CARBO, M., RIERA, D., SAMPOL, B. and HIPOLITO, M., 2004, Understanding down-regulation of photosynthesis under water stress: future prospects and searching for physiological tools for irrigation management. *Annals of Applied Biology*, **144**, pp. 273–283.

FRENCH, A.N., JACOB, F., ANDERSON, M.C., KUSTAS, W.P., TIMMERMANS, W., GIESKE, A., SU, Z., SU, H., MCCABE, M.F., LI, F., PRUEGER, J. and BRUNSELL, N., 2005, Surface energy fluxes with the Advanced Spaceborne Thermal Emission and Reflection Radiometer (ASTER) at the IOWA 2002 SMACEX site (USA). *Remote Sensing of Environment*, **99**, pp. 55–65.

GENUTCHEN, V.M.TH., 1980, A closed–form equation for predicting hydraulic conductivity of unsaturated soils. *Soil Science Society of American Journal*, **44**, pp. 892–898.

GOWARD, S.N., XUE, Y. and CZAJKOWSKI, K.P., 2002, Evaluating land surface moisture conditions from the remotely sensed temperature/vegetation index measurements: an extrapolation with the simplified simple biosphere model. *Remote Sensing of Environment*, **79**, pp. 225–242.

GUPTA, P.L. and SASTRY, P.S.N., 1986, Estimating evapotranspiration from midday canopy temperature. *Irrigation Science*, **7**, pp. 237–243.

GUTMAN, G.G., 1994, Global data on land surface parameters from NOAA AVHRR for use in numerical climate models. *Journal of Climate*, **7**, pp. 669–680.

HALL, F.G., HEUMRICH, K.F., GOETZ, S.J., SELLERS, P.J. and NICKENSON, J.E., 1992, Satellite remote sensing of surface energy balance: success, failure and unresolved issues of FIFE. *Journal of Geophysical Research*, **97**, pp. 19061–19089.

HATFIELD, J.L., WANJURA, D.F. and BARKER, G.L., 1985, Canopy temperature response to water stress under partial canopy. *Transactions of the ASAE*, **28**, pp. 1607–1611.

HOWELL, T.A., TOLK, J.A., SCHNEIDER, A.D. and EVETT, S.R., 1998, Evapotranspiration, yield, and water use efficiency of corn hybrids differing in maturity. *Agronomy Journal*, **90**, pp. 3–9.

JACKSON, R.D., IDSO, S.B., REGINATO, R.J. and PINTER, P.J., 1981, Canopy temperature as a crop water stress index. *Water Resources Research*, **17**, pp. 1133–1138.

JIANG, H., LIU, S., SUN, P., AN, S., ZHOU, G. and LI, C., 2004, The influence of vegetation type on the hydrological process at the landscape scale. *Canadian Journal of Remote Sensing*, **30**, pp. 743–763.

KUSTAS, W., CHOUDHURY, B.J., REGINATO, M.M.R., JACKSON, R., GAY, L. and WEAVER, H., 1989, Determination of sensible heat flux over sparse canopy using thermal infrared data. *Agricultural and Forest Meteorology*, **44**, pp. 197–216.

KUSTAS, W.P., MORAN, M.S., HUMES, K.S., STANNARD, D.I., PINTER, P.J., HIPPS, L.E., SWIATEK, E. and GOODRICH, D.C., 1994, Surface energy balance estimates at local and regional scales using optical remote sensing from an aircraft platform and atmospheric data collected over semiarid rangelands. *Water Resources Research*, **30**, pp. 1241–1260.

IDSO, S.B., JACKSON, R.D., PINTER, P.J, JR, REGINATO, R.J. and HATFIELD, J.L., 1981c, Normalizing stress degree-day for environmental variability. *Agricultural and Forest Meteorology*, **24**, pp. 45–55.

LIANG, S., 2000, Narrowband to broadband conversions of land surface albedo: 1. algorithms. *Remote Sensing of Environment*, **76**, pp. 213–238.

LIANG, S., 2004, Quantitative *Remote Sensing of Land Surfaces* (New York: John Wiley & Sons, Inc.).

MECIKALSKI, J.R., DIAK, G.R., ANDERSON, M.C. and NORMAN, J.M., 1999, Estimating fluxes on continental scales using remotely sensed data in an atmosphere-land exchange model. *Journal of Applied Meteorology*, **38**, pp. 1353–1369.

MORAN, M.S., CLARKE, T.R., INOUE, Y. and VIDAL, A., 1994, Estimating crop water deficit using the relationship between surface-air temperature and spectral vegetation index. *Remote Sensing of Environment*, **49**, pp. 246–263.

NAGLER, P.L., SCOTT, R.L., WESTENBURG, C., CLEVERLY, J.R., GLENN, E.P. and HUETE, A.R., 2005, Evapotranspiration on western U.S. rivers estimated using the Enhanced Vegetation Index from MODIS and data from eddy covariance and Bowen ratio flux towers. *Remote Sensing of Environment*, **97**, pp. 337–351.

NEMANI, R.R., PIERCE, L., RUNNING, S.W. and GOWARD, S.N., 1993, Developing satellite derived estimates of surface moisture status. *Journal of Applied Meteorology*, **32**, pp. 548–557.

NORMAN, J.M., KUSTAS, W.P. and HUMES, K.S., 1995b, A two-source approach for estimating soil and vegetation energy fluxes from observations of directional radiometric surface temperature. *Agricultural and Forest Meteorology*, **77**, pp. 263–293.

NOURBAEVA, G., KAZAMA, S. and SAWAMOTO, M., 2003, Assessment of daily evapotranspiration using remote sensing data. *Environmental Informatics Archives*, **1**, pp. 421–427.

PARODI, G.N., 2000, AVHRR Hydrological Analysis System, 2000, Algorithms and theory. Version 1.0, WRES-ITC, Netherlands.

PARTON, W.J. and LOGAN, J.A., 1981, A model for diurnal variation in soil and air temperature. *Agricultural and Forest Meteorology*, **23**, pp. 205–216.

PRIESTLEY, C.H.B. and TAYLOR, R.J., 1972, On the assessment of surface heat and evaporation using large-scale parameters. *Monthly Weather Review*, **100**, pp. 81–92.

ROBELING, R.A., VAN PUTTEN, E., GENOVESE, G. and ROSEMA, A., 2004, Application of Meteosat derived meteorological information for crop yield predictions in Europe. *International Journal of Remote Sensing*, **25**, pp. 5389–5401.

ROSEMA, A., 1993, Using METEOSAT for operational evapotranspiration and biomass monitoring in the Sahel region. *Remote Sensing of Environment*, **46**, pp. 27–44.

SANDHOLT, I., KJELD, R. and JENS, A., 2002, A simple interpretation of surface temperature/vegetation index space for assessment of surface moisture status. *Remote Sensing of Environment*, **79**, pp. 213–224.

SARVANAAPAVAN, T., DYE, D. and SHIBASAKI, R., 1996, Mid-day atmospheric humidity from thermal infrared observation of the NOAA-14 AVHRR satellite: validation in tropical environment. GIS Development.net, AARS, ACRS, 1996, Oceanography/Meteorology.

SCOTT, C.A., BASTIAANSSEN, W.G.M. and AHMAD, M.D., 2003, Mapping root zone soil moisture using remotely sensed optical imagery. *Journal of Irrigation and Drainage Engineering*, **129**, pp. 326–335.

SEGUIN, B. and ITIER, B., 1983, Using midday surface temperature to estimate daily evaporation from satellite thermal IR data. *International Journal of Remote Sensing*, **4**, pp. 371–383.

SELLERS, P.J., HALL, F.G., ASRAR, G., STREBEL, D.E. and MURPHY, R.E., 1988, The first ISLSCP field experiment (FIFE). *Bulletin of the American Meteorological Society*, **69**, pp. 22–27.

TASUMI, M., 2003, Progress in operational estimation of regional evapotranspiration using satellite imagery. PhD dissertation, University of Idaho, Moscow, Idaho.

VAN DAM, J.C. and MALLIK, R.S. (Eds), 2003, Water productivity of irrigated crops in Sirsa district, India, integration of remote sensing, crop and soil model and geographic information system. WATPRO final report, including CDROM ISBN 90–6464–264–6, 173 pp.

VAN DE GRIEND, A.A. and OWE, M., 1993, On the relationship between thermal emissivity and normalized difference vegetation index for natural surfaces. *International Journal of Remote Sensing*, **14**, pp. 1119–1131.

VERMOTE, E., TANRE, D., DEUZE, J.L., HERMAN, M. and MORCRETTE, J.J., 1997, Second simulation of the satellite signal in the solar spectrum (6S). *6s User Guide version 2*.

VOGT, J.V., NIEMEYER, S. and VIAU, A.A., 2001, Monitoring water stress at regional scales. *Proceedings of the 23rd Canadian Symposium on Remote Sensing*, 21–24 August 2001, Laval University, Sainte Foy, Quebec, Canada, pp. 315–321.

WANG, C., QI, S., NIU, Z. and WANG, J., 2004, Evaluating soil moisture status in China using the temperature-vegetation dryness index (TVDI). *Canadian Journal of Remote Sensing*, **30**, pp. 671–679.